Journal of Engineering Science and Technology
Vol. 8, No. 2 (2013) 141 - 164

EFFECT OF CONVECTIVE BOUNDARY CONDITIONS AT BOTTOM WALL ON NATURAL CONVECTION IN A SQUARE CAVITY

ASWATHA[1,*], C. J. GANGADHARA GOWDA[2], S. N. SRIDHARA[3], K. N. SEETHARAMU[4]

[1]Department of Mechanical Engineering, Bangalore Institute of Technology, Bangalore - 560 004, India
[2]Department of Mechanical Engineering, PES College of Engineering, Mandya-571 401, India
[3]Principal / Director, K. S. School of Engineering and Management, Bangalore - 560 062, India
[4]Department of Mechanical Engineering, PES Institute of Technology, Bangalore-560 085, India
*Corresponding Author: aswath_bit@yahoo.co.in

Abstract

Simulations were carried out for natural convection in a square cavity using finite volume based computational procedure with biased quadratic elements to investigate the influence of convective boundary conditions at bottom wall. Parametric study has been carried out for a wide range of Rayleigh number (Ra) ($10^3 \leq Ra \leq 10^8$), Prandtl number (Pr) ($0.7 \leq Pr \leq 17$) and heat transfer coefficient (h) ($0.1 \leq h \leq 10^4$ W/m^2 K). It is observed from the present study that the heat transfer is primarily due to conduction for Rayleigh number up to 10^4. Convection dominant heat transfer is observed at higher *Ra* values. The intensity of circulation increases with increase in Rayleigh number. The average heat transfer rate at the bottom wall is found to be invariant for all values of heat transfer coefficient for *Ra* up to 10^4. The power law correlations between average Nusselt number and Rayleigh numbers are presented for convection dominated regimes.

Keywords: Natural convection, Cavities, Convective boundary conditions, Prandtl number, Numerical heat transfer.

1. Introduction

The combined convective heat transfer and fluid flow is an important interdisciplinary area in engineering and science such as cooling of electronic components, nuclear reactors, lakes and reservoirs, solar collectors, meteorology,

Nomenclatures

Bi_T	Thermal Biot number
g	Acceleration due to gravity, m/s^2
H	Height of the cavity, m
h	Heat transfer coefficient, W/m^2 K
k	Thermal conductivity, W/m K
L	Length of the cavity, m
Nu	Local Nusselt number
$\overline{Nu}$	Average Nusselt number
p	Dimensional pressure, Pa
p_r	Prandtl number
R^2	Regression coefficient
Ra	Rayleigh number
T	Temperature, K
T_c	Temperature of cold vertical wall, K
T_∞	Ambient temperature, K
u	x- component of velocity, m/s
v	y- component of velocity, m/s

Greek Symbols

α	Thermal diffusivity, m^2/s
β	Volume expansion coefficient, K^{-1}
θ	Dimensionless temperature
γ	Kinematic viscosity, m^2/s
ρ	Density, kg/m^3
ψ	Stream function, m^2/s

Subscripts

b	Bottom wall
S	Side wall
T	Thermal

heat exchangers and crystal growth, prevention of sub-oil water pollution, storage of nuclear waste, etc.

Most of the early investigations of these problems are dealt by Cotton [1], Jaluria [2], Ostrach [3] and Yang [4]. Sarris et al. [5] studied the effect of sinusoidal top wall temperature variations within a square cavity. It has been reported that the sinusoidal wall temperature variation produces uniform melting of metals such as glass. Buoyancy driven flows are complex because of essential coupling between the flow and thermal fields. In particular, internal flow problems are considerably more complex than external ones [6]. Electronic components are usually mounted on the vertical boards which form channels or cavities and the heat generated by the components is removed by a naturally induced flow of air [7]. Enclosures with non-uniform temperature distributions on the walls are dealt by Erenburg et al. [8], Leong et al. [9] and Wakashima and Saitoh [10].

In the literature, investigations on natural convection heat transfer reported that the heat transfer occurs in an enclosure due to the temperature differences across the walls. Eckert and Carlson [11] have studied natural convection between two vertical plates with different temperatures in which the air is used as a working fluid. Heat transfer across the vertical layers is dealt by Emery and Chu [12]. Weinbaum [13] and Ostrach [14] have investigated natural convection in horizontal cylinders. Shallow cavity with differentially heated end walls is dealt by Cormack [15]. The natural convection of air in enclosures or channels either uniformly heated/cooled or discretely heated have received much attention [16, 17]. Basak et al. [6] have reported the effect of temperature boundary conditions (Constant temperature and sinusoidally varying) on the bottom wall for Ra varying from 10^3 to 10^5 for both the Prandtl numbers of 0.7 and 10. The temperature of side walls as well as bottom wall affects the stratification rates and flow patterns [18].

Perusal of prior numerical investigations by Lage and Bejan [19, 20], Nicolette et al. [21], Hall et al. [22], Xia and Murthy [23] reveal that several attempts have been made to acquire a basic understanding of natural convection flows and heat transfer characteristics in enclosures. However, in most of these studies, one vertical wall of the enclosure is cooled and another one heated while the remaining top and bottom walls are insulated. Recently, Lo et al. [24] studied convection in a cavity heated from left vertical wall and cooled from opposite vertical wall with both horizontal walls insulated for temperature thermal boundary conditions using differential quadrature method. Numerical results are reported for several values of both width-to-height aspect ratio of enclosure and Raleigh number. Corcione [25] studied natural convection in a rectangular cavity heated from below and cooled from top as well as sides for variety of thermal boundary conditions. Numerical results are reported for several values of both aspect ratios of enclosure and Rayleigh numbers.

Recently, Oztop [26] numerically studied the mixed convection in a channel with volumetric heat source and different opening ratio at the exit. It is found that the location of the exit opening has strong effect on flow and temperature distribution in the presence of volumetric heat source. Numerical investigations on entropy generation due to natural convection in square cavity with multiple discrete heat sources have been carried by Mukhopadhayay [27]. It has been observed that minimum entropy generation rate was achieved for the same condition at which the minimum peak heater temperature was obtained. Natural convection in a square cavity with a localized non-uniform heat source on the bottom wall was studied by Saravanan and Sivaraj [28]. It is found that for $Gr = 10^6$ non-uniform heating sources enhance the overall heat transfer rate compared to uniform heating of the heat sources whereas for $Gr = 10^7$ its effect is marginal. Eliton et al. [29] studied the buoyancy-driven flow of air in a partially open square 2D cavity with internal heat source. It is concluded that there is a significant influence of the opening on the heat transfer in the cavity.

The present work is based on the Basak et al. [6]. However, Basak et al. [6] have studied the effect of natural convection in a square cavity with uniform and sinusoidal temperature at bottom wall for Ra 10^3 to 10^5 only. It has been observed from the literature that most of the study on natural convection in a cavity is extended up to $Ra = 10^7$ and considered air as a working fluid. However, in the present investigation, the studies are extended for a Prandtl number up to 17. It is

observed from the present literature that no work is carried out on natural convection in a square cavity with convective boundary conditions.

The objective of the present work is to investigate the effect different convective boundary conditions varied from h = 0.1 W/m^{2}K to 10000 W/m^{2}K at the bottom wall, symmetrically cooled side wall and adiabatic top wall for the range of Ra from 10^3 to 10^8 and Pr ranging from 0.7 to 17.

2. Mathematical Formulation

A physical system as illustrated in Fig. 1 is used for simulating natural convective flow and heat transfer characteristics. The cavity of length (L) and height (H) has a bottom wall subjected to convective boundary conditions, two cold vertical walls are at constant temperature T_c and the top wall is adiabatic. The gravitational force is acting downwards. A buoyant flow develops because of thermally induced density gradient. Heat is transferred from the hot wall to cold walls.

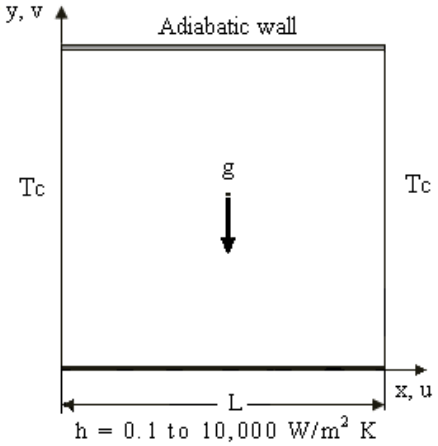

Fig. 1. Geometry of the Cavity.

The governing equations for natural convection flow are conservation of mass, momentum and energy equations and they are written as [6]:

Continuity:
$$\frac{\partial u}{\partial x}+\frac{\partial v}{\partial y}=0 \tag{1}$$

X-momentum:
$$u\frac{\partial u}{\partial x}+v\frac{\partial u}{\partial y}=-\frac{1}{\rho}\frac{\partial p}{\partial x}+\gamma\left(\frac{\partial^2 u}{\partial x^2}+\frac{\partial^2 u}{\partial y^2}\right) \tag{2}$$

Y-momentum:
$$u\frac{\partial v}{\partial x}+v\frac{\partial v}{\partial y}=-\frac{1}{\rho}\frac{\partial p}{\partial y}+\gamma\left(\frac{\partial^2 v}{\partial x^2}+\frac{\partial^2 v}{\partial y^2}\right)+g\beta(T-T_c) \tag{3}$$

Energy:
$$u\frac{\partial T}{\partial x}+v\frac{\partial T}{\partial y}=\alpha\left(\frac{\partial^2 T}{\partial x^2}+\frac{\partial^2 T}{\partial y^2}\right) \tag{4}$$

No-slip boundary conditions are specified at all walls.

Bottom wall: $h(x,0) = 0.1\text{W/m}^2\text{ K to}10{,}000\text{W/m}^2\text{ K}$,

Top wall: $\dfrac{\partial T}{\partial y}(x, H) = 0$ and (5)

Sidewalls: $T(0, y) = T(L, y) = T_c$

The fluid is assumed to be Newtonian and its properties are constant. Only the Boussinesq approximation is invoked for the buoyancy term.

The change of variables is as follows:

$$\theta = \frac{T - T_c}{T_\infty - T_c}, \quad \text{Pr} = \frac{\gamma}{\alpha}, \quad Bi_T = \frac{hL}{k}, \quad \text{Ra} = \frac{g\beta(T_\infty - T_c)L^3\,\text{Pr}}{\gamma^2} \tag{6}$$

In the present investigation, the geometry has been created and discretized using Gambit 2.4. FLUENT CFD package is used to simulate the natural convection of air in cavities.

3. Numerical Procedure

In the present investigation, the set of governing equations are integrated over the control volumes, which produces a set of algebraic equations. The PISO (Pressure Implicit with Splitting of Operators) algorithm developed by Issa [30] is used to solve the coupled system of governing equations. The set of algebraic equations are solved sequentially by ADI (Alternating Direct Implicit) method. A second-order upwind differencing scheme is used for the formulation of the convection contribution to the coefficients in the finite-volume equations. Central differencing is used to discretize the diffusion terms. The computation is terminated when all of the residuals reach below 10^{-5}. The calculations are carried out using the FLUENT commercial code.

4. Stream Function and Nusselt Number

4.1. Stream function

The fluid motion is displayed using the stream function ψ obtained from velocity components u and v. The relationship between stream function, ψ and velocity components for two dimensional flows are given by Batchelor [31]:

$$u = \frac{\partial \psi}{\partial y} \text{ and } v = -\frac{\partial \psi}{\partial x} \tag{7}$$

This leads to a single equation:

$$\frac{\partial^2 \psi}{\partial x^2} + \frac{\partial^2 \psi}{\partial y^2} = \frac{\partial u}{\partial y} - \frac{\partial v}{\partial x} \tag{8}$$

Using the above definition of the stream function stream line plots is made. The positive sign of ψ denotes anticlockwise circulation, and the clockwise circulation is represented by the negative sign of ψ.

4.2. Nusselt number

In order to determine the local Nusselt number, the temperature profiles are fit with quadratic, cubic and bi-quadratic polynomials and their gradients at the walls are determined, where the temperature boundary conditions are specified (cold walls). It has been observed that the temperature gradients at the surface are almost the same for all the polynomials considered. Hence only a cubic fit is made for the temperature profiles to extract the local gradients at the walls to calculate the local heat transfer coefficients from which the local Nusselt numbers are obtained. Integrating the local Nusselt number over each side, the average Nusselt number for each side is obtained as

$$\overline{\mathrm{Nu}_s} = \int_0^H \mathrm{Nu}_s dy \tag{9}$$

Elsherbiny et al. [32] measured natural convection heat transfer in vertical and inclined rectangular cavities where the isothermal sidewalls were at different temperatures and the end walls were perfectly conducting having a linearly varying temperature bounded by the temperature of the sidewalls. From their measurements the following correlation is presented.

$$\overline{Nu} = \max\left\{\left[1+\left(\frac{0.193Ra^{1/4}}{1+\left(1800/Ra\right)^{1.289}}\right)^3\right]^{1/3},\ 0.0605Ra^{1/3}\right\} \tag{10}$$

Abdellah Belkacem et al. [33] have used stream function vorticity formulation to study the natural convection of a square enclosure with sinusoidal protuberance for the Ra up to 10^6 with Pr = 0.71. Sathiyamoorthy et al. [34] have studied the effect of the temperature difference aspect ratio on natural convection in a square cavity for non-uniform thermal boundary conditions for Ra = 10^5 and for various values of Prandtl number varying from 0.01 to 10. Kandaswamy et al. [35] have studied natural convection in a square cavity in the presence of heated plate with two vertical cold walls and two horizontal adiabatic walls, Grashof number ranging from 10^3 to 10^5 for different aspect ratios and position of heated plate for Pr = 0.71.

5. Results and Discussion

5.1. Verification of the present methodology

The grid independent study has been made with different grids and biasing of an element to yield consistent values [24]. The present methodology is compared with Lo et al. [24], in which the authors have studied for Ra = 10^3 to Ra = 10^7, for the cases of uniform temperature at vertical walls and adiabatic horizontal top and bottom walls. Different grid sizes of 31×31, 41×41, 51×51 and 61×61 uniform mesh as well as biasing have been studied. Figure 2(a) shows the convergence of the average Nusselt number at the heated surface with grid refinement for Ra = 10^5 of Lo et al. [24]. The grid 41×41 biasing ratio (BR) of 2 (The ratio of maximum cell to the minimum cell is 2, thus making cells finer near the wall) gave results identical to that of 61×61 uniform mesh. In view of this, 41×41 grid with biasing ratio 2 is used in all further computations. It may be noted that Lo et al. [24] have used a uniform mesh of 31×31 for their study. However, in the

present case, the study has been made for Rayleigh number ranging from Ra = 10^3 to 10^7. Convective boundary conditions have used at the bottom wall. The average Nusselt numbers computed by the present methodology for the values of Ra ranging from 10^3 to 10^7 are compared with that of Lo et al. [24] in Fig. 2(b). The agreement is found to be excellent.

Comparisons with local quantities of interest, such as temperature and velocities have been made with respect to the reference, Basak et al. [6]. In addition the local Nu for both bottom and side walls for various boundary conditions have been calculated. A comparison with available experimental results [32] is also made. The details are furnished below.

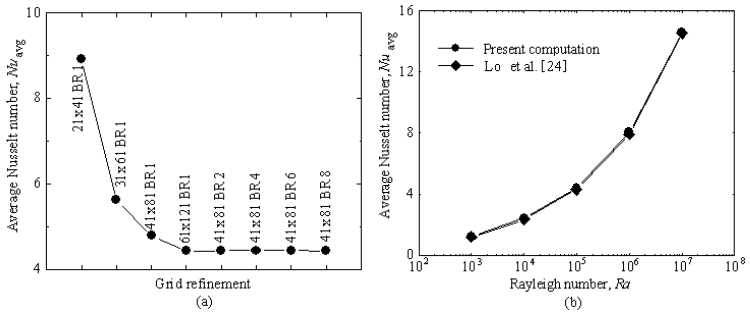

Fig. 2. Convergence of Average Nusselt Number with (a) Grid Refinement (b) Lo et al. [24].

i) Stream functions and temperature profiles

The case of constant wall temperature at the bottom with two cold side walls, identical to the case studied by Basak et al. [6] has been investigated with a view to verify the present methodology.

Figure 3 shows streamlines and temperature profiles of uniform temperature at bottom wall for Ra = 10^5. It is observed that there is a good agreement between results of both Basak et al. [6] (dashed lines) and present one (solid lines). Figure 4 shows streamlines and temperature profile for the case of bottom wall subjected to sinusoidal temperature variation for Ra = 10^5.

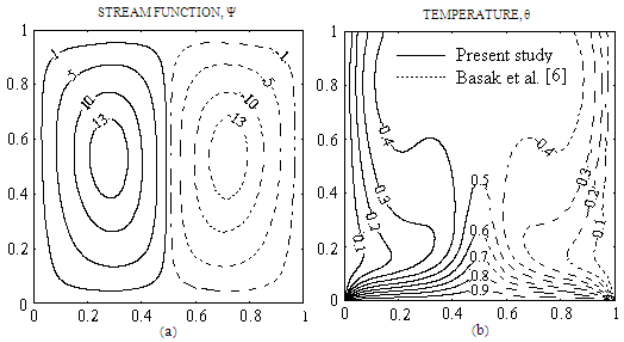

Fig. 3. Streamlines and Temperature Profiles - Constant Temperature on Bottom Wall - Ra = 10^5.

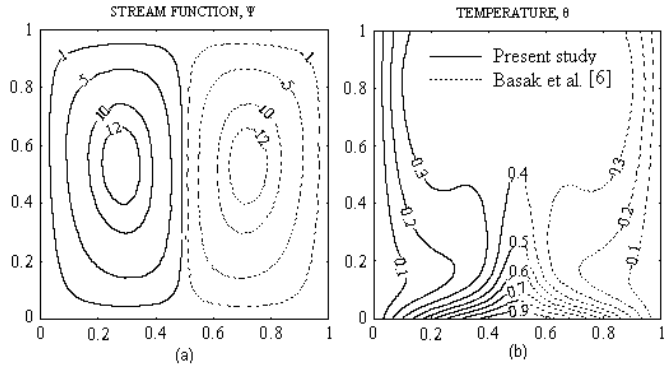

Fig. 4. Streamlines and Temperature Profiles - Sinusoidal Temperature on Bottom Wall - Ra = 10^5.

(ii) Local Nusselt number

Next, the validation of local Nusselt number is considered. Figure 5(a) shows the comparison of local Nusselt number at the bottom wall of the present study with that of Basak et al. [6] for both uniform and sinusoidal temperature variation. It is observed from the Fig. 5(a) that the local Nusselt number at the bottom wall is found to be in excellent agreement with that of Basak et al. [6]. Figure 5(b) shows similar results for the side wall. Again an excellent agreement is observed between the two.

(iii) Average Nusselt number

Next, a comparison of the average Nu for both bottom and side walls are made with that of Basak et al. [6]. Table 1 shows the comparison of variation of average Nusselt number against Rayleigh number for both bottom and side walls for constant temperature and sinusoidal variation at bottom wall. It is observed from the Table 1 that there is good agreement between the present results and that of Basak et al. [6] for both bottom and side walls.

(iv) Verification with experimental results

Published experimental data are not available for the cavity configuration and boundary conditions similar to that undertaken in the present study. Thus, direct validation of the computations against suitable experimental data could not be performed. However, in order to validate the predictive capability and accuracy of the present code, computations are performed using the configuration and boundary conditions of the experiment conducted by Elsherbiny et al. [32]. They measured natural convection heat transfer in vertical and inclined rectangular cavities where the isothermal sidewalls were at different temperatures and the end walls were perfectly conducting having a linearly varying temperature bounded by the temperature of the sidewalls. Computations are performed for one of their vertical cavity configuration with aspect ratio 5 for which they provided the experimental results in the form of a correlation for the average Nusselt number as a function of the Rayleigh number is given in Eq. (10).

The average Nusselt numbers computed by the present code for values of Ra ranging from 10^3 to 10^7 are compared with the correlation of Elsherbiny et al. [32] in Fig. 6. The agreement is found to be excellent with a maximum discrepancy of about 3.5%, which validates the present computations.

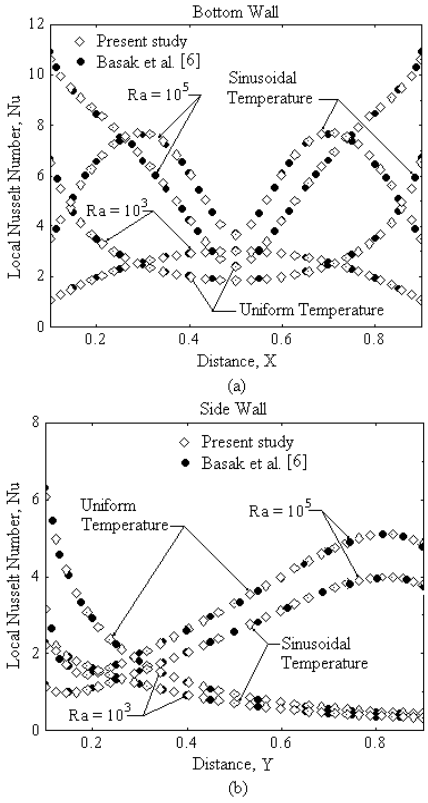

Fig. 5. Comparison of Local *Nu* of Present Study with Basak et al. [6].

Table 1. Comparison of Average Nu with Basak et al. [6].

Ra	Bottom wall						Side wall					
	Uniform Temperature			Sinusoidal Temperature			Uniform Temperature			Sinusoidal Temperature		
	$\overline{Nu}_b$ [6]	Present study	% error	$\overline{Nu}_b$ [6]	Present study	% error	$\overline{Nu}_S$ [6]	Present study	% error	$\overline{Nu}_S$ [6]	Present study	% error
10^3	5.35	5.36	0.12	1.99	2.02	1.56	2.68	2.68	0.00	0.997	0.988	0.92
$5x10^3$	5.62	5.71	1.60	2.78	2.81	1.08	2.80	2.85	1.79	1.390	1.405	1.08
10^4	6.15	6.26	1.73	3.45	3.52	2.03	3.06	3.12	1.86	1.700	1.720	1.18
10^5	8.66	8.68	0.23	5.15	5.26	2.19	4.30	4.29	0.24	2.530	2.505	0.98

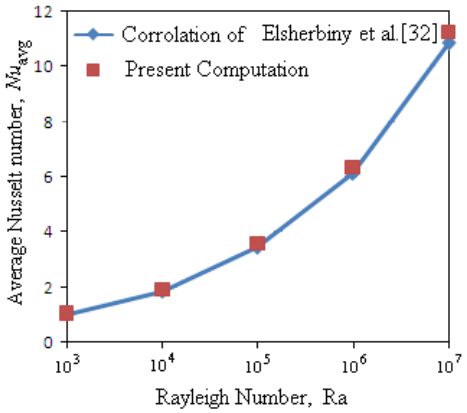

Fig. 6. Comparison of Present Average Nusselt Number with that of Elsherbiney et al. [32].

5.2. Convective boundary conditions

In this study the convective heat transfer takes place at the bottom wall, top wall is adiabatic and symmetrically cooled vertical wall is investigated. The heat transfer co-efficient (h) varied from 1 W/m^{2}K to 10,000 W/m^{2}K. The fluid flow and heat transfer characteristics in cavities are studied for range of Rayleigh number from 10^3 to 10^8. The Prandtl number varied from 0.7 to 17. Also, the investigations are carried out by interchanging the boundary conditions of cold walls and convective bottom wall for a particular case.

5.3. Effect of heat transfer coefficient (h)

The cavity, which is used for the analysis is subjected to convective boundary conditions at the bottom wall. Computations are carried out for convective heat transfer coefficient ranging from 1 W/m^{2}K to 10,000 W/m^{2}K. Figure 7 illustrates the variation of temperature along the bottom wall for heat transfer coefficient 'h'. The temperature variations along the bottom wall for conduction dominated heat transfer, i.e., for Ra = 10^3 is as shown in Fig. 7(a). It has been observed that the variation of temperature takes place for the value of 'h' from 1 W/m^{2}K to 50 W/m^{2}K. The contours are smooth curves and spreading entire span of the bottom wall. The temperature contours for h > 50 W/m^2 K is almost overlapping. The major portions of the curves are almost parallel to the horizontal wall except near the cold walls for larger values of 'h'. This is due conduction domination for Ra = 10^3. Figures 7(b) and (c) show the variations of temperature along the bottom wall for Ra = 10^5 and 10^7 respectively. The maximum temperature occurs at the centre of the bottom wall as expected. It is observed that in the present study, the temperature contours are smooth curves in the convection dominated region and they are steeper near the cold wall as shown in Fig. 7(b). Figure 7(c) shows for Ra = 10^7, in contrary to Ra = 10^5 there is small drop of temperature along the bottom wall. However, the variations near the cold wall are very small compared to that of Ra = 10^5.

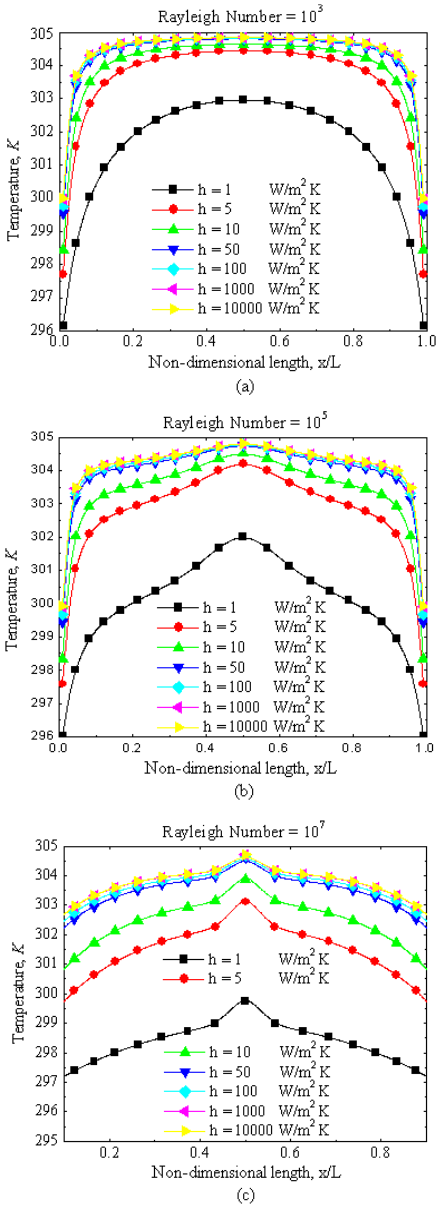

Fig. 7. Bottom Wall Temperatures for Different Heat Transfer Coefficient Boundary Conditions (a) Ra =10^3, (b) Ra =10^5 and (c) Ra = 10^7, AR = 1.

Figures 8 and 9 illustrate the stream function and isotherm contours for Ra = 10^5 and 10^7 when bottom wall is exposed to convective environment. It has been observed that for Ra = 10^5 the magnitudes of stream function for h = 1 W/m^2 K are lower (ψ = 12) than for h = 5 W/m^2 K. However, these values remains same, i.e., ψ = 12 up to h = 100 W/m^{2}K. But, it has increased to 16 for

$h \geq 1000$ W/m^{2}K. It is observed from Fig. 8(a) that for $h = 5$ W/m^{2}K, the outer cells of the stream functions are concentrated near the walls of the cavity as compared to $h = 1$ W/m^{2}K. However, the central cells are settled at the vertical centre but size increases for the range of h varied from 5 W/m^{2}K to 100 W/m^{2}K. For $h \geq 1000$ W/m^{2}K the magnitude of the central cells increased to 16 being smaller in size.

Figures 8(a), 8(b) and 8(c) show the temperature contours of $h = 1$, 5, 10, 50, 100 and 10,000 W/m^{2}K for Ra = 10^5. For $h = 1$ W/m^{2}K, the temperature profiles are smooth curves and spread for the bottom wall up to $\theta = 0.3$ (70%). The contours are symmetric about vertical line at the centre of bottom wall and are settling nearer to bottom wall. It is observed from Fig. 8(a) that, if $h \geq 5$ W/m^2 K the discontinuities exists at the bottom corners, which are similar to constant temperature cases. The temperature profiles $\theta \leq 0.4$ are symmetric about vertical walls. These contours are moving towards the cold vertical walls with increase of 'h'. The contours remain unchanged for $h \geq 100$ W/m^{2}K.

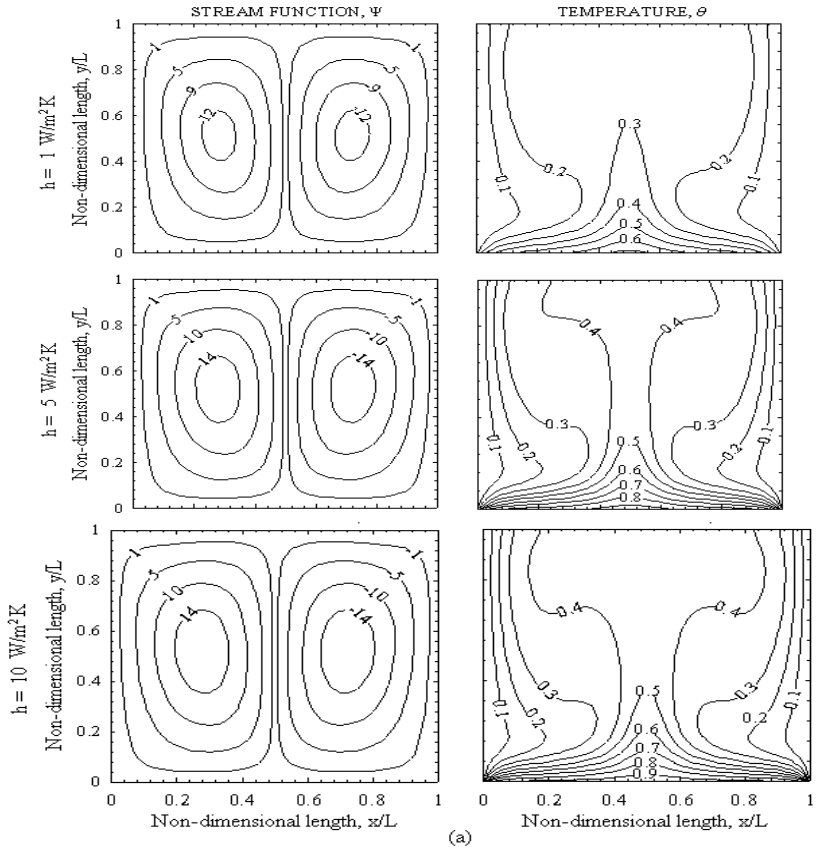

Fig. 8(a). Stream Functions and Temperature Contour Plots for Bottom Wall Subjected to Convective Boundary Condition with h = 1, 5 and 10 W/m^2 K for Ra = 10^5.

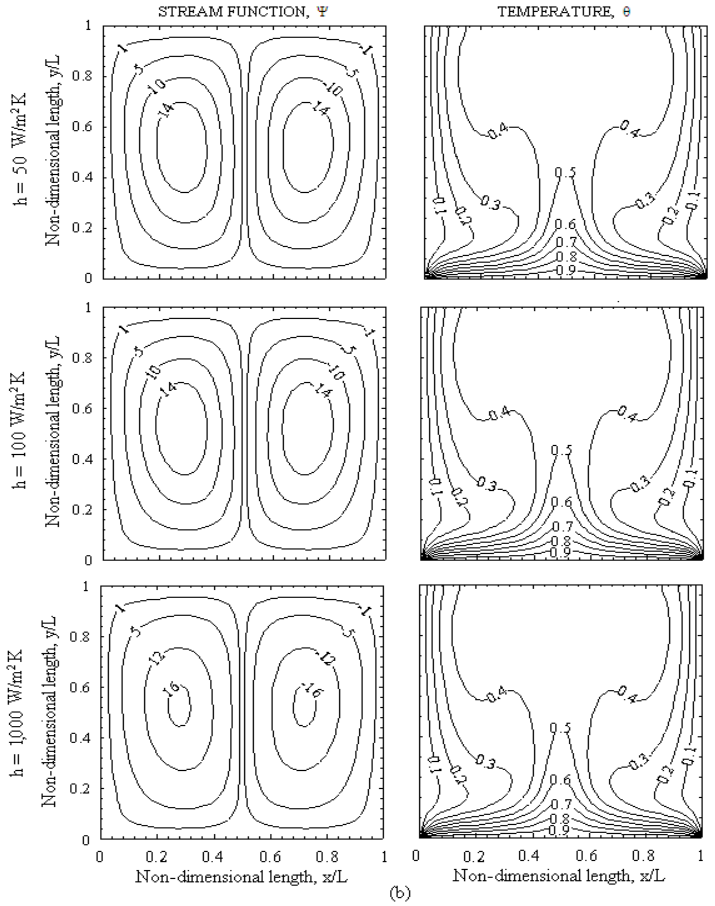

Fig. 8(b). Stream Functions and Temperature Contour Plots for Bottom Wall Subjected to Convective Boundary Condition with h = 50, 100 and 1,000 W/m^2 K for Ra = 10^5.

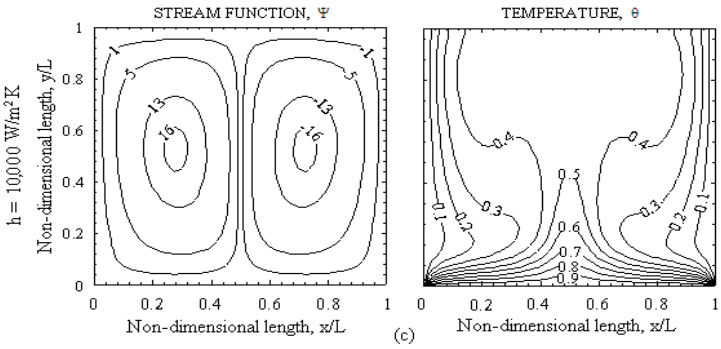

Fig. 8(c). Stream Functions and Temperature Contour Plots for Bottom Wall Subjected to Convective Boundary Condition with h = 10,000 W/m^2 K for Ra = 10^5.

Figures 9 show the stream functions and temperature profiles for Ra = 10^7. The magnitude of the stream functions remains unchanged irrespective of variations of the values of heat transfer coefficient. However, the small variations in the size of the central cells up to h = 10 W/m^2 K and it remains unchanged for $h \geq$ 10 W/m^2 K. The temperature contours plotted for Ra = 10^7 are also shown in Fig. 9. The temperature contours for $\theta \geq 0.3$are smooth curves for h = 1 W/m^{2}K. Temperature curves tend to concentrate towards the cold vertical walls for heat transfer coefficient (h) up to 1,000 W/m^2 K and it remains unchanged for $h \geq$ 1,000 W/m^2 K.

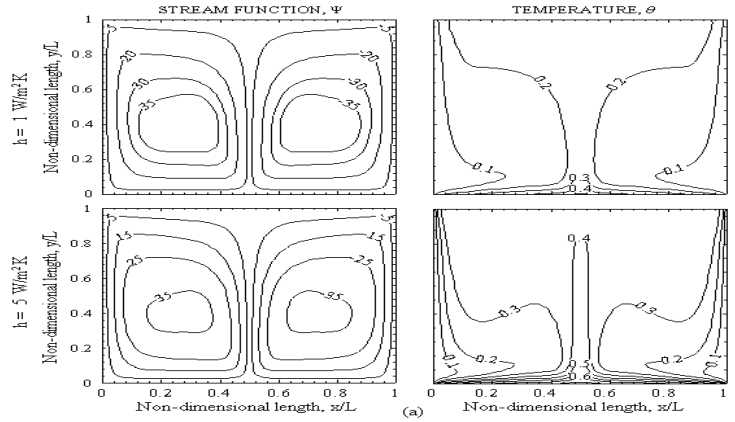

Fig. 9(a). Stream Functions and Temperature Contour Plots for Bottom Wall Subjected to Convective Boundary Condition with h = 1and 5 W/m^2 K for Ra=10^7.

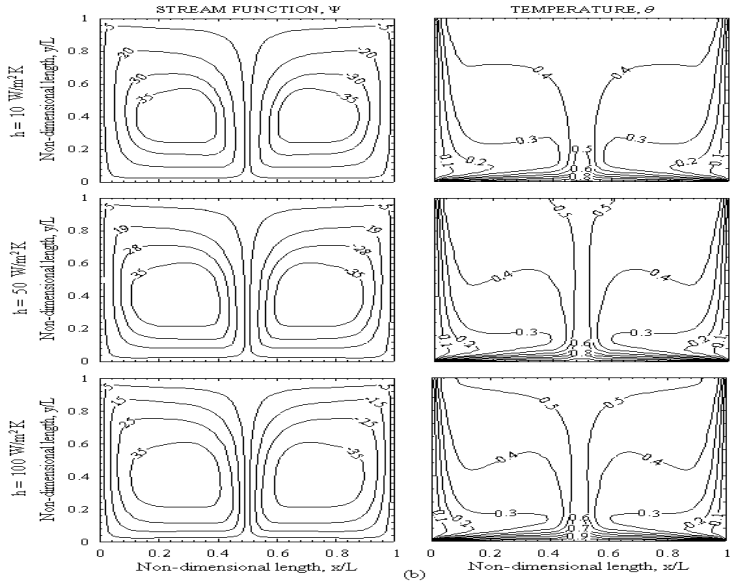

Fig. 9(b). Stream Functions and Temperature Contour Plots for Bottom Wall Subjected to Convective Boundary Condition with h = 10, 50 and 100 W/m^2 K for Ra = 10^7.

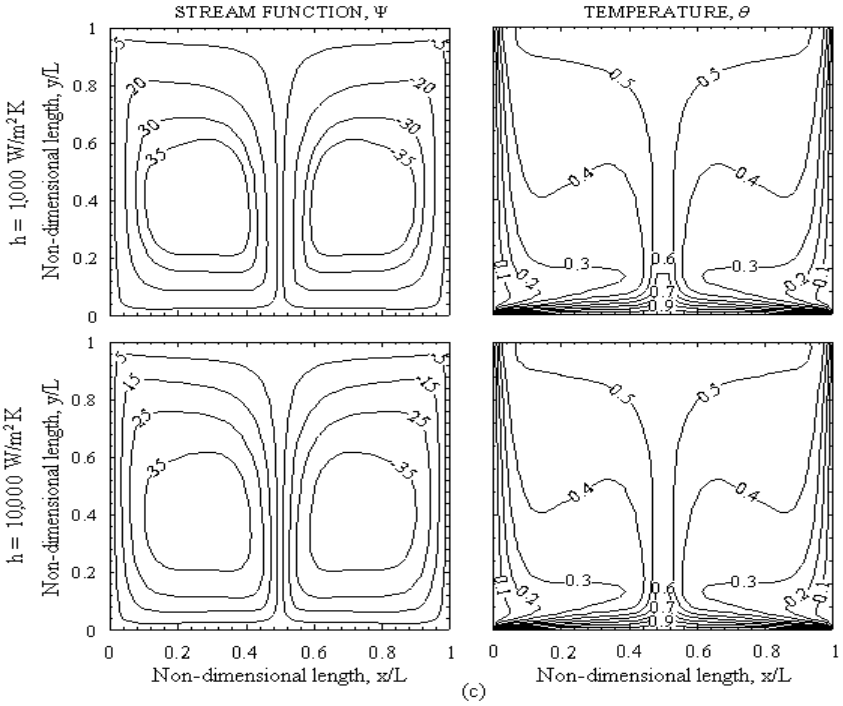

Fig. 9(c). Stream Functions and Temperature Contour Plots for Bottom Wall Subjected to Convective Boundary Condition with h = 1,000 and 10,000 W/m^2 K for Ra = 10^7.

Figures 10(a), (b) and (c) show the variation of local Nusselt number for side walls. Figure 10(a) shows the variations of local Nusselt number for Ra = 10^3. The local Nusselt numbers monotonically decreases along the side wall for the range of values of heat transfer coefficients, h, studied. This is mainly due to conduction dominated heat transfer. However, for h = 1 W/m^2 K the local Nusselt numbers are lower than other values at all the points. For $h \geq 5$ W/m^2 K the local Nusselt number is almost same except some little variations near the bottom wall.

Variation of local Nusselt numbers for Ra = 10^5 shown in Fig. 10(b). It has been observed that, the variations of local Nusselt numbers decreases along the side wall for Y = 0.2, then increases up to Y = 0.8 and again decreased. These changes happened at the corners because of decrease of velocity magnitude due to change of direction of fluid. However, it is observed that local Nusselt number increases with increase of heat transfer coefficient at all the points up to 50 W/m^2 K. For $h \geq 50$ W/m^2 K the variations of local Nusselt numbers are almost same along the side wall.

Figure 10(c) shows the variations of local Nusselt numbers along the side wall for Ra = 10^7. In contrast of Ra = 10^5, the local Nusselt numbers increases monotonically along the length of the side wall for Ra = 10^7. It is observed that the increased magnitude of the stream function increases the heat transfer rate even at the corners also.

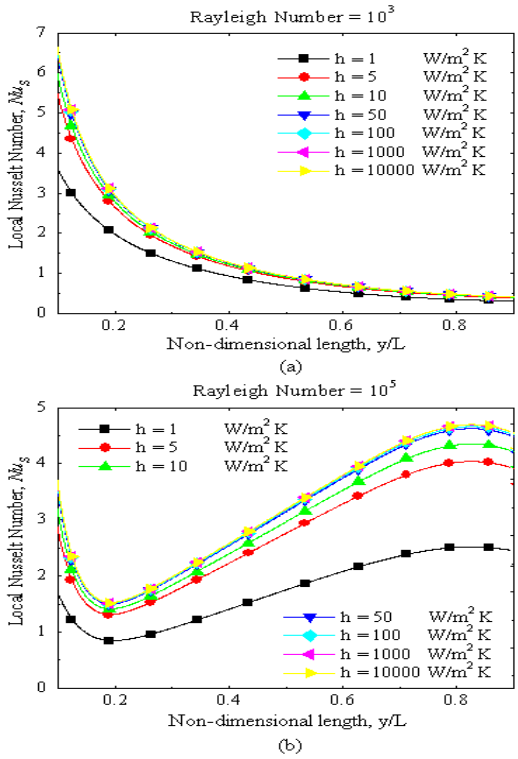

Fig. 10(a) and (b). Variation of Local Nusselt Numbers at Side Wall for Different Convective Boundary Conditions for Rayleigh Number 10^3 and 10^5.

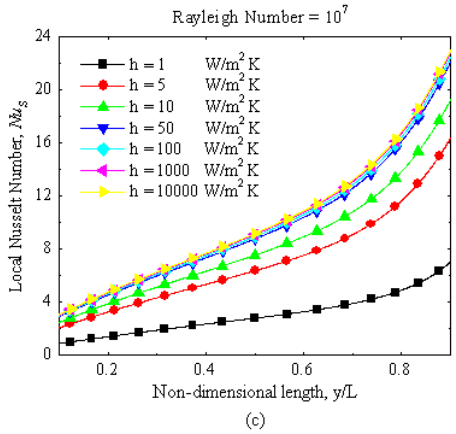

Fig. 10(c). Variation of Local Nusselt Numbers at Side Wall for Different Convective Boundary Conditions for Rayleigh Number 10^7.

Figure 11 shows the variation of average Nusselt number for the case of convective cases for side walls. It can be observed that the average Nusselt

number increases with Rayleigh number as expected. The average Nusselt numbers do not show any change with h beyond $h \geq 50$ W/m^2 K.

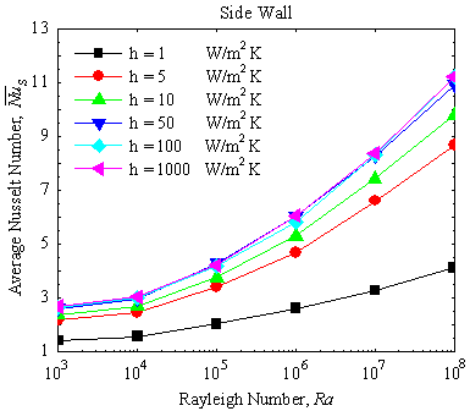

Fig. 11. Variations of Average Nusselt number for Side Wall for Different Convective Boundary Conditions at Bottom Wall with Pr = 0.7.

5.4. Effect of Rayleigh number

The cavity used for the analysis is subjected to convective boundary conditions ranging from 1 W/m^2 K to 10,000 W/m^2 K at the bottom wall. Computations are carried out for Rayleigh number ranging from 10^3 to 10^8. It has been observed from the previous sections that the variations of temperature contours, stream functions, local and average Nusselt numbers, etc. take place for heat transfer coefficient $h \leq 50$ W/m^2 K. In the present investigations the effect of Rayleigh number and cavity aspect ratio have been studied by considering $h = 100$ W/m^2 K.

Figure 12 illustrates the temperature distribution along the bottom wall for Rayleigh number ranging from 10^3 to 10^7. It has been observed that, as the Rayleigh number increases the temperature at all the points along the length decreased. However the temperature is significantly decreased at the centre of the bottom wall.

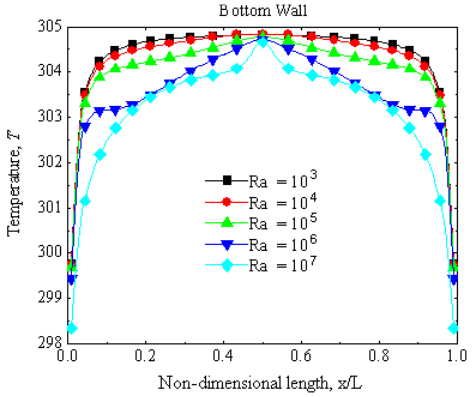

Fig. 12. Variations of Temperature for Rayleigh Number Ranging from 10^3 to 10^7 for h = 100 W/m^2 K.

Figure 13 illustrates the stream function and isotherm contours for Ra = 10^3 - 10^7 with the bottom wall exposed to h = 100 W/m^2 K. It has been observed that for Ra = 10^3 the magnitudes of stream function are very low (ψ = 0.01 to 0.2) and the heat transfer is primarily due to conduction. During conduction dominant heat transfer, the temperature contours are similar and occur symmetrically. The temperature contour θ = 0.1 is opened and occurs symmetric with vertical cold walls. The temperature contours, θ = 0.2 and above are smooth curves and are generally symmetric with respect to vertical centre line. The temperature contours remain invariant up to Ra < 5×10^3 (not shown). However, it is observed from Fig. 13 that, the magnitude of stream function increases with increase of Rayleigh number up to 10^6. For Ra = 10^4 and 10^5 central cells are located at the centre of vertical line and are elliptical in shape. However, for Ra = 10^6 the central cells move vertically. For Ra = 10^7 the cells are concentrating towards the cold walls, which results in the increase of the size of the cells. The central cells are moved towards bottom wall.

Since, the convection effect becomes more for Ra $\geq 5\times10^3$, the temperature profiles are spread for the entire span of the bottom wall up to θ = 0.5 (60%). The contours are symmetric about vertical line and are settling nearer to bottom wall for Ra up to 10^6. The temperature profiles θ = 0.4 and below get distorted towards side walls. For Ra = 10^7, the temperature profiles are spread for the entire span of the bottom wall up to θ = 0.6. The curves θ = 0.3 and lower values are concentrating nearer to the vertical cold walls.

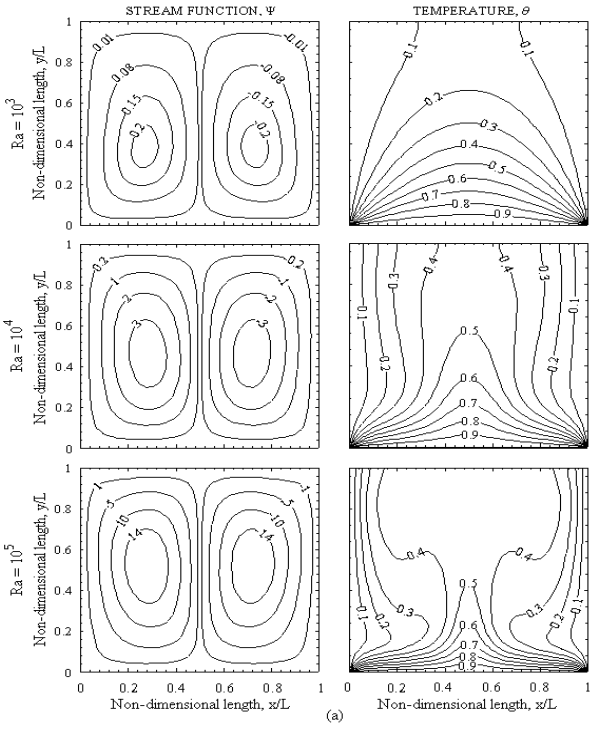

Fig. 13(a). Streamlines and Temperature Profiles for h = 100 W/m^2 K on Bottom Wall for Rayleigh Number Ra = 10^3, 10^4 and 10^5.

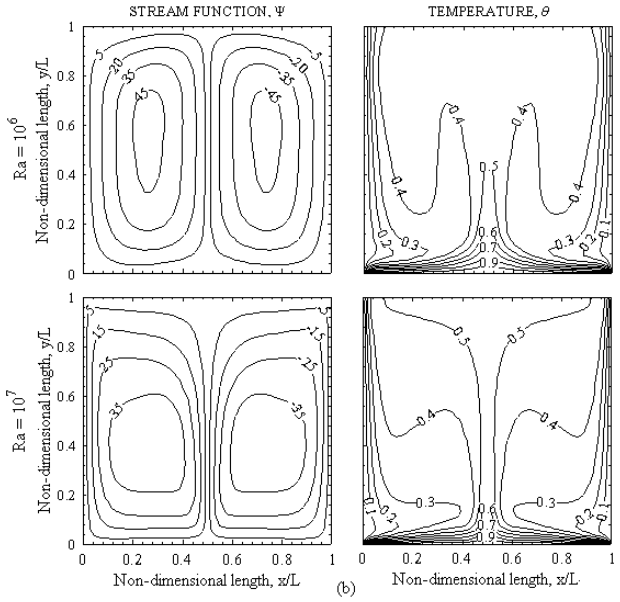

Fig. 13(b). Streamlines and Temperature Profiles for h = 100 W/m^2 K on Bottom Wall for Rayleigh Number Ra = 10^6 and 10^7.

Figure 14 shows the variation of local Nusselt number for side walls. The investigations have been carried for Rayleigh number ranging from 10^3 to 10^7 for h = 100 W/m^2 K. It has been observed that for Ra = 10^3 the local Nusselt number is monotonically decreasing along the side wall due to conduction domination heat transfer. In convection dominated region, as the Rayleigh number increases the non-uniformity of the local Nusselt number at the side wall increases. As expected, the local Nusselt number at any given location increases with Rayleigh number. For Ra = 10^6 the local Nusselt number increased and decreased at Y = 0.8. But, the local Nusselt number increased linearly up to Y = 0.7 and increased more steeply for Ra = 10^7.

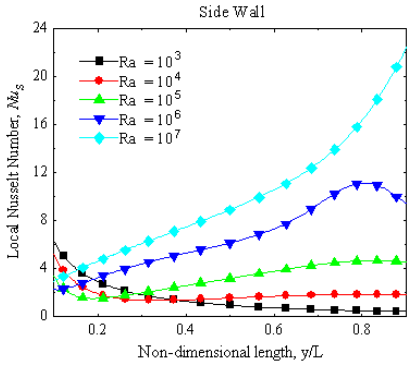

Fig. 14. Variation of Local Nusselt Number on Side Wall for Rayleigh Number Ranging from 10^3 to 10^7 for Bottom Wall Subjected to Heat Transfer Coefficient h = 100 W/m^2 K.

5.5. Effect of Prandtl number

Figure 15 shows the variation of average Nusselt number for the case of h = 100 W/m^2 K for side wall with Prandtl number Pr = 0.7, 6.08 and 17.08. It can be observed that the average Nusselt number increases with Rayleigh number for Pr studied as expected, for Ra > 10^6. However, average Nusselt number for Pr = 6.08 and 17.08 are lesser than Pr = 0.7 for Rayleigh number up to 10^6.

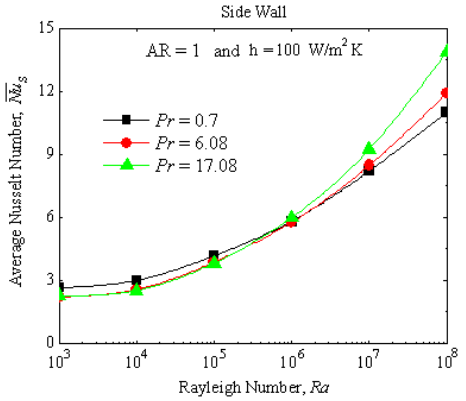

Fig. 15. Variation of Average Nusselt Number at Side Wall in a Square Cavity for Different Pr with h = 100 W/m^2 K.

5.6. Variations of Biot number

Figure 16 shows the average Nusselt number variation with the Biot number. As the Biot number (heat transfer coefficient) increases, the Nusselt number increases and reaches an asymptotic value equal to the Nusselt number value obtained with the constant temperature boundary condition for a given Ra, as expected.

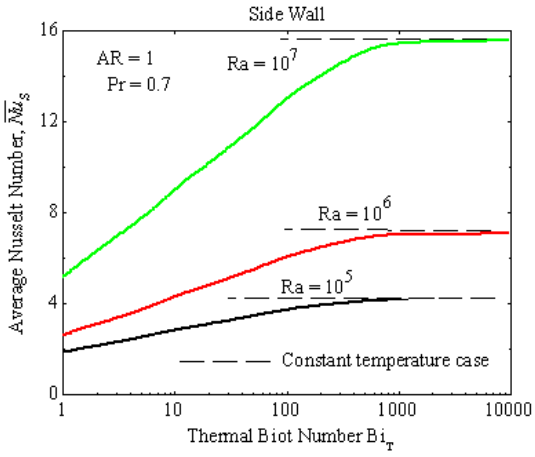

Fig. 16. Average Nusselt Number Variation with Thermal Biot Number for Different Rayleigh Numbers.

Figure 17 shows the variations of non-dimensional temperature at the bottom wall. It can be observed that as Bi_T increases, the temperature at the bottom wall will tend to be more uniform. Simultaneously as Bi_T increases, it will approach a non-dimensional temperature of 1.0 at the bottom wall.

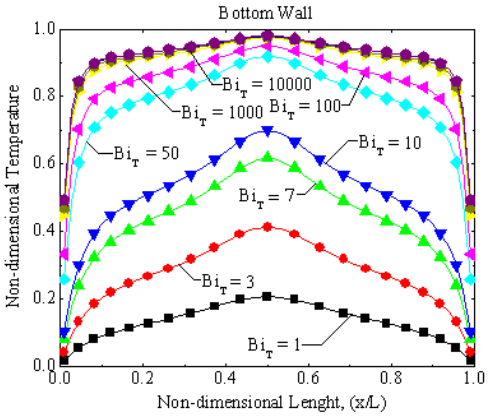

Fig. 17. Non-dimensional Temperature Variation with Thermal Biot Number at Bottom Wall for Ra = 10^5.

Table 2. Correlations of Average Nusselt Number with Rayleigh Number for a Square Cavity.

Prandtl number (*Pr*)	Rayleigh (*Ra*) number range	*h* W/m^{2}K	Side wall		
			Correlation	R^2	% Error
0.7	10^4 to 10^8	1	$\overline{Nu_s} = 0.596\,Ra^{0.105}$	0.998	< 0.30
		5	$\overline{Nu_s} = 0.689\,Ra^{0.138}$	0.998	< 0.30
		10	$\overline{Nu_s} = 0.738\,Ra^{0.141}$	0.998	< 0.25
		50	$\overline{Nu_s} = 0.755\,Ra^{0.149}$	0.998	< 0.20
		100	$\overline{Nu_s} = 0.808\,Ra^{0.142}$	0.999	< 0.20
		1000	$\overline{Nu_s} = 0.788\,Ra^{0.146}$	0.999	< 0.20
6.08	10^4 to 10^8	1	$\overline{Nu_s} = 0.330\,Ra^{0.147}$	0.998	< 0.25
		5	$\overline{Nu_s} = 0.294\,Ra^{0.175}$	0.999	< 0.25
		10	$\overline{Nu_s} = 0.366\,Ra^{0.165}$	0.998	< 0.30
		50	$\overline{Nu_s} = 449\,Ra^{0.177}$	0.999	< 0.20
		100	$\overline{Nu_s} = 0.555\,Ra^{0.167}$	0.998	< 0.30
		1000	$\overline{Nu_s} = 0.717\,Ra^{0.158}$	0.998	< 0.35
17.08	10^4 to 10^8	1	$\overline{Nu_s} = 0.305\,Ra^{0.153}$	0.998	< 0.30
		5	$\overline{Nu_s} = 0.291\,Ra^{0.176}$	0.999	< 0.20
		10	$\overline{Nu_s} = 0.379\,Ra^{0.165}$	0.998	< 0.30
		50	$\overline{Nu_s} = 0.477\,Ra^{0.171}$	0.998	< 0.25
		100	$\overline{Nu_s} = 0.446\,Ra^{0.187}$	0.998	< 0.35
		1000	$\overline{Nu_s} = 0.589\,Ra^{0.172}$	0.998	< 0.36

The investigations have been carried out for h=1, 5, 10, 50, 100, 1000 and 10000 W/m^2 K for the range of Ra and Pr = 0.7, 6.08 and 17.08. Table 2 shows the correlations and error involved for side wall. The range of convection domination is same for different Prandtl number and this occurred at Ra $\leq 10^4$. In order to use the study carried out here for practical purposes, correlations are developed between average Nusselt number and Rayleigh numbers. In the present study, the maximum error involved in correlating average Nusselt number with Rayleigh number is less than 0.4% in the range of Ra = 10^4 to 10^8.

6. Conclusions

The effect of different convective boundary conditions for the values of h ranging from 1 W/m^2 K to 10,000 W/m^2 K at the bottom wall is studied. The top wall is adiabatic and side walls are maintained at constant temperature. The following conclusions have been observed during the present study.

- It is observed that the heat transfer characteristics like temperature variations along the bottom wall, non-dimensional temperature profiles, stream functions in a cavity, Local and average Nusselt numbers along the cold walls remains same for h > 50 W/m^2 K.
- The contours of stream functions and isotherms are symmetric about centre vertical line of bottom wall.
- The average Nusselt number increases monotonically with increase of both Ra for side wall.
- It is observed that the average Nusselt number is less for higher Prandtl number for Ra $\leq 10^6$, but it is more for Ra $\geq 10^6$.
- It is observed that as the Biot number increases, the Nusselt number increases and reaches an asymptotic value obtained with the constant temperature boundary condition for a given Ra.

References

1. Cotton, I. (1978). Natural convection in enclosures. *Proceedings of the 6th International Heat Transfer Conference, Toronto*, Vol. 6, 13-43.
2. Jaluria, Y. (1980). *Natural convection heat and mass transfer*. Pergamon, Oxford, 209-235.
3. Ostrach, S. (1988). Natural convection in enclosures. *Journal of Heat Transfer*, 110(4b), 1175-1190.
4. Yang, K.T. (1988). Transitions and bifurcations in laminar buoyant flows in confined enclosures. *Journal of Heat Transfer,* 110(4b), 1191-1204.
5. Sarris, I.E.; Lekakis, I.; and Vlachos, N.S. (2002). Natural convection in a 2D enclosure with sinusoidal upper wall temperature. *Numerical Heat Transfer, Part A*, 42(5), 513-530.
6. Basak, T.; Roy, S.; and Balakrishnan, A.R. (2006). Effect of thermal boundary conditions on natural convection flows with in a square cavity. *International Journal of Heat and Mass Transfer*, 49(23-24), 4525-4535.

7. Dehghan, A.A.; and Behnia, M. (1996). Combined natural convection-conduction and radiation heat transfer in a discretely heated open cavity. *Journal of Heat Transfer*, *Transactions of ASME*, 118(1), 56-64.
8. Erenburg, V.; Gelfgat, A.Y.; Kit, E.; Bar-Yoseph, P.Z.; and Solan, A. (2003). Multiple states, stability and bifurcations of natural convection in a rectangular cavity with partially heated vertical walls. *Journal of Fluid Mechanics*, 492, 63-89.
9. Leong, W.H.; Hollands, K.G.T.; and Brunger, A.P. (1999). Experimental Nusselt numbers for a cubical-cavity benchmark problem in natural convection. *International Journal of Heat and Mass Transfer*, 42(11), 1979-1989.
10. Wakashima, S.; and Saitoh, T.S. (2004). Benchmark solutions for natural convection in a cubic cavity using the high-order time-space methods. *International Journal of Heat and Mass Transfer*, 47(4), 853-864.
11. Eckert, E.R.G.; and Carlson, W.O. (1961). Natural convection in an air layer enclosed between two vertical plates with different temperatures. *International Journal of Heat and Mass Transfer*, 2(1-2), 106-120.
12. Emery, N.; and Chu, C. (1965). Heat transfer across vertical layers. *Journal of Heat Transfer*, 87, 110-114.
13. Weinbaum, S. (1964). Natural convection in horizontal cylinders. *Journal of Fluid Mechanics*, 18(3), 409-448.
14. Brooks, I.H.; and Ostrach, S. (1970). An experimental investigation of natural convection in a horizontal cylinder. *Journal of Fluid Mechanics*, 44(3), 545-561.
15. Cormack, D.E.; Leal, L. G.; and Seinfeld, J.H. (1974). Natural convection in shallow cavity with differentially heated end walls. Part 2, Numerical solutions. *Journal of Fluid Mechanics*, 652, 231-246.
16. Chadwick, L.; Webb, B.M.; and Ricci, R. (1991). Experimental and Numerical investigations on natural convection from two dimensional discrete heat sources in a rectangular enclosure. *International Journal of Heat and Mass Transfer*, 34(7), 1679-1693.
17. Ahmed, G.R.; and Yovanovich, M.M. (1991). Influence of discrete heat source location on convection heat transfer in a vertical square enclosure. *ASME Journal Electronic Packaging*, 113(3), 268-274.
18. Dixit, H.N.; and Babu, V. (2006). Simulation of high Rayleigh number natural convection in a square cavity using the lattice Boltzmann method. *International Journal of Heat and Mass Transfer*, 49(3-4), 727-739.
19. Lage, J.L.; and Bejan, A. (1991). The Ra - Pr domain of laminar natural convection in an enclosure heated from the sides. *Numerical Heat Transfer Part A*, 19(1), 21-41.
20. Lage, J.L.; and Bejan, A. (1993). The resonance of natural convection in an enclosure heated periodically from the side. *International Journal of Heat and Mass Transfer*, 36(8), 2027-2038.
21. Nicolette, V.F.; Yang, K.T.; and Lloyd, J.R. (1985). Transient cooling by natural convection in a two-dimensional square enclosure. *International Journal of Heat and Mass Transfer*, 28(9), 1721-1732.

22. Hall, J.D.; Bejan, A.; and Chaddock, J.B. (1988). Transient natural convection in a rectangular enclosure with one heated side wall. *International Journal of Heat and Fluid Flow*, 9(4), 396-404.
23. Xia, C.; and Murthy, J.Y. (2002). Buoyancy-driven flow transitions in deep cavities heated from below. *Journal Heat Transfer*, 124(4), 650-659.
24. Lo, D.C.; Young, D.L.; and Tsai, C.C. (2007). High resolution of 2D natural convection in a Cavity by the DQ method. *Journal of Computational and Applied Mathematics*, 203(1), 219-236.
25. Corcione, M. (2003). Effects of the thermal boundary conditions at the sidewalls upon natural convection in rectangular enclosures heated from below and cooled from above. *International Journal of Thermal Sciences*, 42(2), 199-208.
26. Oztop, H.F. (2010). Influence of exit opening location on mixed convection in a channel with volumetric heat source. *International Communications in Heat and Mass Transfer*, 37(4), 410-415.
27. Mukhopadhayay, A. (2010). Analysis of entropy generation due to natural convection in square enclosure with multiple discrete heat source. *International Communications in Heat and Mass Transfer*, 37(7), 867-872.
28. Saravanan, S.; Sivaraj. C. (2011). Natural convection in an enclosure with a localized non-uniform heat source on the bottom wall. *International Journal of Heat and Mass Transfer*, 54(13-14), 2820 - 2828.
29. Fontana, E.; da. Silva, A.; Mariana, V.C. (2011). Natural convection in a partially open square cavity with internal heat source: An analysis of the opening mass flow. *International Journal Heat and Mass Transfer*, 54(7-8), 1369 - 1386.
30. Issa, R.I. (1985) Solution of the implicitly discretized fluid flow equations by operator-splitting. *Journal of Computational Physics*, 62(1), 40-65.
31. Batchelor, G.K. (1993). *An introduction to fluid dynamics*. Cambridge University Press, Cambridge, UK.
32. Elsherbiny, S.M.; Raithby, G.D.; and Hollands, K.G.T. (1982). Heat transfer by natural convection across vertical and inclined air layers. *Journal Heat Transfer*, 104(1), 96-102.
33. Belkacem, A.; Omar, H.; and Mebrouk, R. (2006). Stream function/vorticity formulation to study the cavity flows by unstructured grid method. *International Journal of Applied Engineering Research*, 1(3), 315-329.
34. Sathiyamoorthy, M.; Basak, T.; Roy, S.; and Mahanti, N.C. (2007). Effect of the temperature difference aspect ratio on natural convection in a square cavity for non-uniform thermal boundary conditions. *Journal Heat Transfer*, 129(12), 1723-1728.
35. Kandaswamy, P.; Lee, J.; and Abdul Hakeem, A.K. (2007). Natural convection in a square cavity in the presence of heated plate. *Nonlinear Analysis: Modelling and Control*, 12(2), 203-212.